Monitoring Measurement Noise Variance for High Integrity Navigation with Cycle Resolution

Samer Khanafseh and Boris Pervan, *Illinois Institute of Technology*

ABSTRACT

In this paper, a methodology is developed to ensure the integrity of high accuracy carrier phase navigation systems that require cycle resolution, given that the measurement noise characteristics might change under different environments. For demanding aviation applications such as autonomous shipboard landing or autonomous airborne refueling, accuracy and integrity of carrier phase positioning and cycle resolution are essential. In such applications, the estimate error covariance matrix is used to assess the quality of cycle resolution as well as the integrity risk of the subsequent position solution. Therefore, any changes in the noise characteristics must be properly accounted for in the integrity risk computation. In this work, a monitor that detects sudden increases in the noise variance is proposed along with an explicit quantification of its effect on integrity risk.

INTRODUCTION

Least squares estimators and Kalman filters guarantee a bounded estimate error variance provided that the measurement errors can be accurately modeled as white noise processes with a variance greater than or equal to the actual variance. The assumed value of the measurement noise standard deviation (or sigma) is used by the navigation algorithm to estimate position and compute protection levels. Nominal values of sigma can be obtained from a prior analysis of data collected over several hours, days, or even months. The data length is primarily dependent on how much noise variation must be encompassed. For example, in the Local Area Augmentation System (LAAS), data is collected over months to capture the impact of non-Gaussian errors, sample size effects, seasonal variations, group delays, and phase center variations on the measurement noise distribution [1]. However, such an analysis can never properly account for all possible antenna environments that may be encountered. The potential danger is that sudden changes in the surroundings (for example weather debris) could lead to situations where the true measurement noise standard deviation exceeds the nominal value used in the estimator. If unaccounted for, these situations can ultimately lead to optimistic protection levels which jeopardize the system integrity risk. Furthermore, in applications that require cycle resolution, the computed probability of correct fix may also become meaningless, which will impact the integrity risk of cycle resolution.

In response, a monitor is needed to continuously verify that the actual measurement error variances are equal to or lower than the nominal variances. However, changes cannot be detected instantaneously because estimating a meaningful standard deviation requires a large number of samples. If the navigation algorithm computes protection levels using the nominal variance, these undetected changes in the measurement noise characteristics will pose an integrity threat. In previous work, we proposed using a Cumulative Sum (CUSUM) monitor to detect variance variations that exceed the nominal value [2]. The CUSUM monitor was used because it has been proven to provide the shortest mean time to detect (MTTD) in the presence of a variance change. The performance of the CUSUM monitor depends on the magnitude of the fault (variance shift ratio) and in most cases, the detection is far from instantaneous. Therefore, the navigation algorithm must use an inflated variance (relative to the nominal value) which allows sufficient time for the CUSUM monitor to detect these changes while guaranteeing meaningful protection levels. Qualitatively, the inflated variance is chosen to provide acceptable levels of both availability and probability of missed detection.

In [2], we provided a derivation that relates integrity risk to the inflation factor, the minimum detectable variance, MTTD, and the mean time between failures (MTBF). A ‘failure’ in this context is the event where the actual measurement noise standard deviation exceeds the nominal value. That derivation was used to impose requirements on the MTTD and the minimum detectable

variance of the monitor for given integrity risk allocations, MTBFs and inflation factors; the allowable inflation factor being driven by availability. The conclusion of the previous work was that for a fixed MTBF, no monitor can detect variance shifts fast enough to meet aviation level requirements unless MTBF is very large. In addition, derivations provided in the previous work were only applicable for float estimation of cycle ambiguities. Given that cycle resolution (fixing) is required for high accuracy applications, and that the probability of correct fix is related to the measurement noise covariance matrix, a new approach is necessary to quantify variance monitor requirements.

In this paper, we propose new approaches to address the MTBF issue by exploiting the fact that, in reality, MTBF varies with fault size. (Extremely large variance increases will be less frequent than smaller increases.) The result of this approach is a required MTBF curve that depends on the fault size. This requirement on MTBF is used as requirements on antenna siting, design, and environment. We also address the cycle resolution issue by rederiving the relation between MTBF, MTTD, fault and bound ratios and the integrity risk requirement.

CUSUM VARIANCE MONITOR

In order to monitor the variance it is necessary to extract the measurement noise, *v*, which can be accomplished several ways. For example, in dual frequency applications, the ionosphere-free code-minus-carrier operation can be used to extract the noise in the code measurements. Once the measurement noise has been extracted from the measurements, several methods are available to detect variance shifts [3-7].

One intuitive method is to estimate the variance (or standard deviation) directly from *v*. Although estimating the variance is straightforward and its distribution is known to be chi-squared with one degree of freedom, the number of samples required to obtain a reliable variance estimate is considerably large. For example, [3] claims that at least 18 independent samples are required to reliably estimate the variance. Therefore, if we assume that the multipath autocorrelation time constant is on the order of 100 seconds, one hour would be required to have a reliable estimate of the variance (18 independent measurements at 200 sec apart, where measurements at two time constants apart are assumed to be independent). Also, it has been shown in [3, 5] that the performance of the Cumulative Sum (CUSUM) monitor is generally better than that of the direct variance estimator. Therefore, the CUSUM monitor is considered in this work.

CUSUM monitoring was introduced in the 1940's by Wald [6], and uses a log-likelihood ratio test to detect mean and variance shifts. It is widely used in quality control, operational research, and manufacturing engineering. Lee and Pullen [3-5] proposed using the CUSUM monitor to detect mean and variance shifts in GPS reference receiver measurements (B-values) for LAAS. For those interested in the theoretical background of the CUSUM monitor and its design, they are referred to [6, 7].

The variance monitor test statistic of the CUSUM for any observable Y_m is [6]:

$$C_m^+(j) = \max\left(0\,,\, C_m^+(j-1) + Y_m(j) - k_\sigma^+\right) \tag{1}$$

The initial value for C^+ can either be 0 (standard CUSUM) or any other value as a fraction of the threshold (Fast Initial Response (FIR) CUSUM). For variance shift detection, the observable for satellite *m* at epoch *j* is the weighted square of the measurement noise $v_m(j)$ (2).

$$Y_m(j) = \left(\frac{v_m(j) - \mu_v}{\sigma_{n,m}}\right)^2 \tag{2}$$

where μ_v is the mean of v_m and $\sigma_{n,m}$ is the nominal standard deviation of v_m. GPS measurement noise is usually assumed to have zero mean, and therefore, (2) can be simplified to:

$$Y_m(j) = \left(\frac{v_m(j)}{\sigma_{n,m}}\right)^2 \tag{3}$$

The constant k_σ^+ in (1) is derived based on the designed value for the detection variance as:

$$k_\sigma^+ = 2\left(\sigma_t / \sigma_n\right)^2 \frac{\ln\left(\sigma_t / \sigma_n\right)}{\left(\sigma_t / \sigma_n\right)^2 - 1} \tag{4}$$

The derivation of this formula can be found in [6]. In [2], we designed the CUSUM monitor for a fault ratio of 2 ($\sigma_t / \sigma_n = 2$ in Equation 4), which results in $k_\sigma^+ = 1.848$.

The CUSUM monitor alarms when the test statistic C_m^+ exceeds a threshold *T*. The threshold for the CUSUM is computed based on the assumption that the observables Y_m (and hence the measurement noise v_m) are independent. However, due to multipath, measurement noise is correlated. As a rule of thumb, measurements taken at twice the multipath autocorrelation time constant can be assumed to be independent. In this work, we assume a time constant of 100 sec for multipath, implying independence for measurements taken 200 sec apart. When the input observables to the CUSUM are independent, C_m^+ becomes a Markov process. In Markov

processes, the current state is only dependent on the previous state. Therefore, the MTTD for the CUSUM monitor is computed using the transition matrix for the Markov process in conjunction with properties of Markov chains. That said, the MTTD computation is still an iterative process. The details behind the computation of MTTD can be found in [6, 7]. To define the threshold, the required probability of false alarm (1×10^{-6} in this paper) that meets an example continuity requirement is used to compute T as 30. With k_σ^+ and T determined, the CUSUM monitor design is complete and its performance can be quantified.

In order to quantify the performance of this CUSUM monitor, different MTTDs are computed for different fault ratios (σ_t/σ_n) ranging from 1.2 to 7. The resultant MTTDs from the CUSUM for these values of fault ratios was presented in [2] and is shown in Figure 1. It is clear that the monitor detects large faults in approximately 600 seconds (3 independent epochs) while requiring many hours to detect smaller faults. The integrity risk of the navigation system must comply with the requirements even if the monitor takes time to detect such faults. The proposed idea is to inflate the variance that the system uses to compute the integrity risk (or protection levels) in order to grant the monitor the required time to detect these faults. In [2] and in the following section, we derive a formula to relate the inflated variance (σ_b) to the integrity risk requirements and the monitor MTTD.

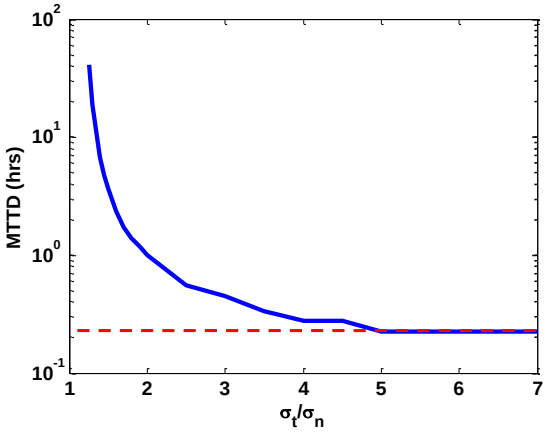

Figure 1: Performance of the designed CUSUM monitor for different fault ratios σ_t/σ_n.

INTEGRITY RISK

Before discussing the monitor design in detail, it is instructive to introduce some fundamental concepts that will be used repeatedly throughout this paper. The fault-free integrity risk is defined as the probability of the coordinate estimate error δx exceeding the alert limit ℓ:

$$I_{H0} = P\left\{ \left| \delta x \right| > \ell \right\} \tag{5}$$

Equivalently, the notion of a protection level occurs frequently in aviation applications, and it is defined as a statistical bound on the estimate error. It resembles (5) where ℓ is replaced by PL and I_{H0} is replaced by the requirement I_{H0req}. Under fault-free conditions, it can be computed by multiplying the standard deviation of the coordinate estimate error σ_x (coming from the estimator) by an integrity factor k_{ff}, that is derived from the required fault-free integrity risk, I_{H0req} (6, 7).

$$PL = k_{ff}\ \sigma_x \tag{6}$$

where k_{ff} is determined from I_{H0req} through the relation

$$k_{ff} = \Phi^{-1}\left(\frac{I_{H0req}}{2} \right) \tag{7}$$

and Φ is the cumulative distribution function for a standard normal random variable.

Although this paper is concerned with anomalous conditions (and hence not fault-free), we still use (6) to construct the PL. Because σ_x is computed using an inflated measurement noise standard deviation, σ_b^2, (6) remains valid for a certain amount of time even if a sudden increase in the true measurement noise standard deviation, σ_t^2, has occurred. It is important to note that σ_b^2 is only used to grant the monitor time to detect if σ_t^2 is larger than the nominal value, σ_n^2. Therefore, the monitor test statistic and threshold are solely based on σ_t^2 and σ_n^2 respectively.

In the case of variance monitoring, a hazardously misleading information (HMI) situation occurs if σ_t^2 exceeds σ_n^2, the monitor's test statistic is less than the threshold and therefore did not detect the anomaly, and the true estimate error exceeded the protection level (defined as the event S). Mathematically, the probability of HMI can be expressed as:

$$P(HMI, S) = P\left\{ \left|\delta x(\sigma_t)\right| > PL(\sigma_b)\ ,\ q(\sigma_t) < T(\sigma_n)\ ,\ S \right\} \tag{8}$$

First, we expand Equation (8) using the low of total probability

$$P(HMI, S) = P\left\{ \left|\delta x(\sigma_t)\right| > PL(\sigma_b)\ ,\ q(\sigma_t) < T(\sigma_n) \mid S \right\} P\left\{ S \right\} \tag{9}$$

In order to simplify the first term on the right hand side of (9), we assume that the event where the estimate error exceeds the protection level and the event where the test statistic is less than the threshold are statistically independent. This assumption is valid if the test statistic is computed using a measurement that is one independent epoch delayed from the current measurement that is used in the estimation of *x*. This delay has already been accounted for in MTTD (by increasing it by the period of one independent epoch) for the monitor as shown in Figure 1. With that assumption, (9) becomes,

$$P(HMI,S)=P\left\{\left|\delta x(\sigma_t)\right|>PL(\sigma_b)\mid S\right\} P\left\{q(\sigma_t)<T(\sigma_n)\mid S\right\}P\left\{S\right\} \quad (10)$$

The second and third terms in the previous equation represent the probability of missed detection (PMD). In this work we treat the PMD as a state probability such that the system is either in the state of $q < T$ and $\sigma_t > \sigma_n$ or not. This probability has a binomial distribution that can be represented as a function of the failure rate (or MTBF in our case) and exposure time (MTTD). This probability is evaluated using the exponential function as:

$$P\left\{q(\sigma_t)<T(\sigma_n),\ S(\sigma_t>\sigma_n)\right\}=1-e^{-\frac{MTTD}{MTBF}} \quad (11)$$

In [2], we derived a closed form, geometry-free expression for a least squares estimate that overbounds the first term on the right hand side of (10) as,

$$P\left\{\left|\delta x(\sigma_t)\right|>PL(\sigma_b)\mid S\right\}\le 2Q\left(\frac{k_{fftd}\ \min_i\left(\sigma_{b,i}/\sigma_{n,i}\right)}{\max_i\left(\sigma_{t,i}/\sigma_{n,i}\right)}\right) \quad (12)$$

where *Q* is the Gaussian tail probability function and *i* is the satellite measurement index.

If the position estimation algorithm relies on cycle resolution a similar geometry-free expression cannot be derived. In this case, the hypothesis that the cycle ambiguities have been fixed incorrectly must be taken into account. Therefore, using the law of total probability and assuming that all incorrect fixes cause the position estimate error to exceed the protection level, the first term in (10) can be expanded, as shown in [8], as,

$$P\left\{\left|\delta x(\sigma_{b,t})\right|>PL(\sigma_b)\mid S\right\}= P\left\{\left|\delta x(\sigma_{b,t})\right|>PL(\sigma_b)\mid S,CF\right\}P_{CF|S}(\sigma_{b,t}) + \left(1-P_{CF|S}(\sigma_{b,t})\right) \quad (13)$$

where $P_{CF|S}$ is evaluated as [9]:

$$P_{CF|S}=\prod_{i=1}^{m(\sigma_b)}\left[2\Phi\left(\frac{1}{2\sigma_{i|I}(\sigma_t)}\right)-1\right] \quad (14)$$

where $\sigma^2_{i|I}$ is the i^{th} conditional variance, which is defined as the variance of the ambiguity *i* conditioned on the previous ambiguities in the set $I = \{1,2,\ldots,i\text{-}1\}$ being fixed correctly. $\sigma^2_{i|I}$ is related to the true measurement error standard deviation (σ_t). It is extracted as the (*i*,*i*) element of the diagonal matrix **D** resulting from the $\mathbf{LDL}^{\mathrm{T}}$ decomposition of the floating cycle ambiguity estimate error covariance matrix. *m* is the number of fixed cycle ambiguities, which is determined by the fault free fixing algorithm and dominated by the inflated variance σ_b. Finally, Φ is defined as $\Phi(x)=\int_{-\infty}^{x}\frac{1}{\sqrt{2\pi}}\exp\left(-\frac{1}{2}v^2\right)dv$.

Notice that the position estimate error is not only influenced by the true measurement error variance σ_t, as in the float estimate, but also by σ_b. – the latter because the number of fixed ambiguities is decided by P_{CF} meeting the integrity risk requirements. P_{CF}, as equation (10) shows, is directly influenced by σ_b.

Because of the complicated nature of equations (13) and (14), the same process that was used to eliminate the geometry in (12) fails for (13). As a result, the first probability term in the right hand side of (13) must be evaluated for different geometries. In [2], having *PL* in (10) helped eliminate the geometry. Since $P\left\{\left|\delta x(\sigma_t)\right|>PL(\sigma_b)\mid S\right\}$ will be evaluated for different geometries, and because $\boldsymbol{\ell}$ for fault-free available geometries is larger than *PL*, exchanging the *PL* by the alert limit $\boldsymbol{\ell}$ in (13) provides is less conservative. Combining (10), (11) and (13) results in

$$P(HMI,S)= \left(1-e^{\frac{-MTTD}{MTBF}}\right)\left[P\left\{\left|\delta x(\sigma_{b,t})\right|>\ell\mid S,CF\right\}P_{CF|S}(\sigma_{b,t}) + \left(1-P_{CF|S}(\sigma_{b,t})\right)\right] \quad (15)$$

Equation (15) can also be modified to fit more complicated algorithms that compute tight bounds on the integrity risk of cycle resolution, such as EPIC [8].

Combining (10) and (12) then substituting the integrity risk budget for the sigma monitor $P(HMI,S)_{req}$ in place of $P(HMI,S)$, we can solve for the required MTBF ($MTBF_{req}$) as,

$$MTBF_{req}(\sigma_{b,t}) = \frac{MTTD(\sigma_t/\sigma_n)}{\ln\left(\frac{P\{|\delta x(\sigma_{b,t})| > \ell \mid S\}}{P\{|\delta x(\sigma_{b,t})| > \ell \mid S\} - P\{HMI, S\}_{req}}\right)} \quad (16)$$

$MTBF_{req}$ in (16) is a function of satellite geometry and the values of σ_b/σ_n and σ_t/σ_n. MTTD in (16) is extracted from Figure 2 for the associated value of σ_t/σ_n and we assume 10^{-7} budget for the variance shift monitor [2]. The goal is to set reasonable requirements on MTBF that the ground station uses as a guideline in siting the antennas. Considering all geometries for all constellations at all locations is not practical and will not (by itself) guarantee integrity. Instead, we first simulate geometries based on a single satellite constellation [10] and location (West Atlantic: 37°N and 74°W). Guaranteeing the airborne integrity under variance shifts for different locations or constellations will be discussed in the following section.

$MTBF_{req}$ in (16) is computed for σ_t/σ_n values of 1.2 to 7 and σ_b/σ_n values of 1.25, 1.5 and 1.75. The resultant $MTBF_{req}$ in Figure 2 is then selected as the maximum $MTBF_{req}$ over all simulated geometries at each σ_t/σ_n value and for the same σ_b/σ_n. Figure 2 shows that as σ_b/σ_n increases, $MTBF_{req}$ decreases, which is less demanding for siting the reference station antennas. However, increasing σ_b/σ_n increases the predicted fault free integrity risk (or protection level), which degrades availability. Therefore, the choice of σ_b/σ_n should be determined by the availability requirement (an example is presented later).

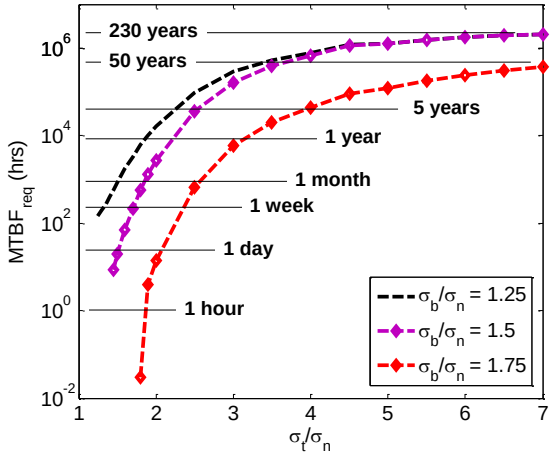

Figure 2: Required MTBF for different values of σ_b/σ_n and σ_t/σ_n

BOUNDING INTEGRITY RISK

As discussed earlier, the CUSUM and MTBF curves alone do not guarantee any specific integrity risk for the airborne system. The integrity risk must be evaluated at the aircraft given its current geometry. The aircraft assumes that the ship meets the $MTBF_{req}$ curve associated with σ_b/σ_n and is using a CUSUM monitor with MTTD curve (Figure 1). Given these assumptions, the aircraft computes a prior probability on the fault P^*, defined in (17) below.

$$P^*(\sigma_{b,t}) = P\{q < T, S\} = \left(1 - e^{-\frac{MTTD(\sigma_t)}{MTBFreq(\sigma_{b,t})}}\right) \quad (17)$$

For example, Figure 3 shows P^* for σ_b/σ_n of 1.5. Practically, this prior probability curve can be stored in the aircraft and used by the airborne system to test its current geometry and compute the variance-monitor integrity risk as

$$P\{HMI, S\}_{comp}(\sigma_{b,t}) = P\{|\delta x(\sigma_{b,t})| > \ell \mid S\} P^*(\sigma_{b,t}) \quad (18)$$

The term $P\{|\delta x(\sigma_{b,t})| > \ell \mid S\}$ in (18) is computed at the aircraft based on its current satellite geometry for different σ_t/σ_n values (Figure 3). Since (18) results in different $P\{HMI,S\}$ values for different σ_t/σ_n, the resultant $P\{HMI|S\}_{max}$ is selected as the maximum value (19):

$$P\{HMI, S\}_{Max} = \max_{\sigma_t/\sigma_n}\left[P\{|\delta x(\sigma_{b,t})| > \ell \mid S\} P^*(\sigma_{b,t})\right] \quad (19)$$

If it is desired that airborne algorithm computes a protection level instead, a similar approach can be followed by computing different PL values for different σ_t/σ_n by solving for PL in (20):

$$\frac{P\{HMI, S\}_{req}}{P^*(\sigma_{b,t})} = P\{|\delta x(\sigma_{b,t})| > PL(\sigma_{b,t}) \mid S\} \quad (20)$$

If cycle resolution is used (13) can be used to substitute the right hand side in (20) as

$$P\{|\delta x(\sigma_{b,t})| > PL(\sigma_b) \mid S, CF\} = \frac{P\{HMI, S\}_{req} - (1 - P_{CF|S}(\sigma_{b,t}))P^*(\sigma_{b,t})}{P^*(\sigma_{b,t})\, P_{CF|S}(\sigma_{b,t})} \quad (21)$$

Similar to computing a fault free protection level (Equations 6 and 7), we use the probability in (21) to compute a probability multiplier k_σ as in (22) and a protection level PL_σ as in (23). The maximum in (23) is due to computing different protection levels for different σ_t/σ_n.

$$k_{\sigma}\left(\sigma_{b,t}\right)=\Phi^{-1}\left(\frac{P\left\{\left|\delta x(\sigma_{b,t})\right|>PL(\sigma_b)\,|\,S,CF\right\}}{2}\right) \quad (22)$$

$$PL_{\sigma}=\max_{\sigma_t/\sigma_n}\left[k_{\sigma}\left(\sigma_{b,t}\right)\cdot\sigma_x\right] \quad (23)$$

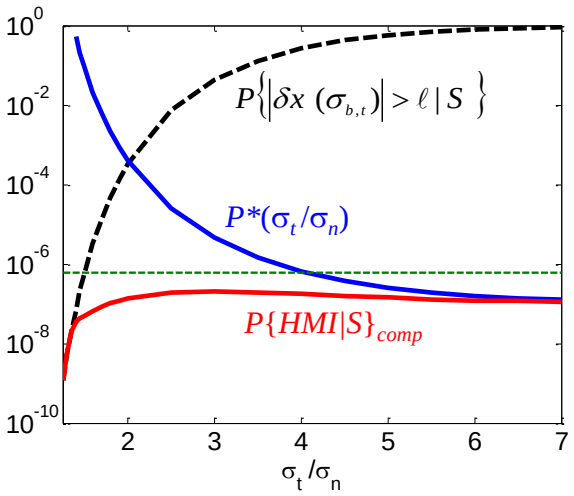

Figure 3: Probability terms of Equation (18) for different values of σ_t/σ_n and σ_b/σ_n=1.5

NAVIGATION APPLICATION EXAMPLE

For example, consider autonomous shipboard landing as an example application. Because of the mobility of the reference station in a shipboard-relative landing application, higher levels of accuracy are required than for similar precision approach applications at land-based airfields. In this work, we use the navigation algorithm that has been developed and detailed in [11-13].

These algorithms perform geometry-free/divergence-free code-carrier filtering continuously for visible satellites on both the aircraft and the ship until the aircraft is close to the ship [11]. Geometry-free filtering [14], by definition, does not depend on the geometry of the satellites or the user location and eliminates major error sources such as atmospheric errors, clock and ephemeris errors and leaves relatively small errors such as receiver noise and multipath. A geometry free measurement of the widelane cycle ambiguity is formed by subtracting the narrowlane pseudorange from the widelane carrier [14, 15]. A drawback of the geometry free measurement is the presence of higher noise caused by the combination of L1 and L2 carrier phase measurements. This drawback can be overcome by filtering the geometry free measurement over time prior to the final approach. In order to model colored multipath noise in the geometry free measurements, a first order Gauss-Markov measurement error model is used. In this work, a time constant of one minute for the ship and 30 seconds for aircraft is assumed.

The outputs of the filtering process are the floating widelane cycle ambiguity estimates. When the aircraft is close to the ship, floating widelane cycle ambiguity estimates can be estimated accurately with the aid of satellite geometric redundancy [11-13,16] and are then fixed subject to the integrity risk requirements.

Before evaluating the availability of the variance monitor, we must select a reasonable value of σ_b/σ_n. Therefore, an availability sensitivity analysis is conducted for different σ_b/σ_n values. The goal is to find the largest value of σ_b/σ_n that has negligible impact on availability. This analysis is conducted for a single aircraft approach by covariance analysis. To account for the GPS satellite geometry change, the availability analysis is performed by simulating 1440 approaches (one approach per minute during the day). In this work, a straight-in approach (Case-III landing approach) is assumed. A given approach is said to be available if the integrity requirements are satisfied at each point along the approach. Availability is calculated as the percentage of approaches for which *VPL* during the entire approach is lower than *VAL*.

In this work, the requirements and simulation parameters are based on those given in [13,16]. The nominal standard deviation (σ_n) of the raw carrier phase measurement noise is assumed to be 5 mm and the nominal standard deviation (σ_n) of the raw pseudorange measurement noise is assumed to be 25 cm. Also, geometry-free prefiltering is assumed to start at the beginning of the approach and is used to generate floating estimates of the widelane cycle ambiguities. The rest of the simulation parameters are summarized in Table I.

Table I: Example Simulation Parameters

Parameter	**Nominal Value**
I_{H0req}	6×10^{-7}
St.dev. of raw code, raw carrier	25 cm, 0.5 cm
Constellation (almanac)	24 SV (DO-229) [10]
Location	37^{o} North, 74^{o} West
Elevation angle mask	10^{o}
VAL at touchdown	1.5 m

Using the simulation parameters in Table I, Figure 4 shows the resulting impact of σ_b/σ_n on the availability. The figure illustrates for this example, that for σ_b/σ_n >1.5 availability degrades drastically. Referring to Figure 2, the antenna placement on the ship (reference station in this example) must meet the MTBF requirement curve for σ_b/σ_n=1.5. For example, the curve suggests that small variance shifts should at least be in the order of days. Therefore, it cannot be placed on the ship deck where

airplane traffic, personnel, and maintenance crew make the multipath environment continuously varying, which implies that σ_t/σ_n might exceed 1.2 multiple times a day. In contrast, if the antennas are placed on the ship mast, they will be less likely to cause σ_t/σ_n to exceed 1. This is especially true for larger σ_t/σ_n assuming that human access is limited to scheduled (or rare) maintenance visits and that the environment quite hardly ever changes.

Using σ_b/σ_n=1.5, the P^* curve in Figure 3 is considered and integrity risk in (19) is computed. We simulate the impact of the variance monitor on availability for different constellations and geometries (but $MTBF_{req}$ is still based on the baseline constellation and geometry used to generate Figure 2). To simulate differences in constellation, one satellite is removed from the constellation at each epoch. The removed satellite is selected such that it results in the worst case constellation (the one that results in the worst Dilution of Precision (DOP)). In addition to the constellation change, ten different locations for the reference station have been used. The resultant availability for each of these simulations matched the fault free case (shown in Figure 4 for σ_b/σ_n=1.5). Therefore, the variance monitor has no impact on availability for the example application and simulated cases. In the future, we will consider simulating depleted constellations with satellite outage model to get more representative availability.

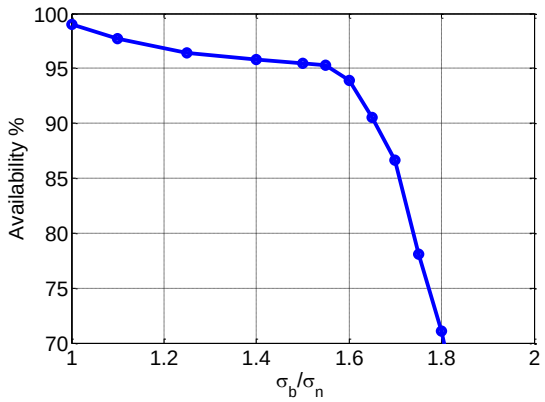

Figure 4: availability for an example application (shipboard landing) for different values of σ_b/σ_n

CONCLUSIONS

In this paper, we developed a method to quantify the integrity risk of measurement variance shifts for navigation architectures that rely on cycle resolution. First, we designed a CUSUM monitor that detects variance shifts with the shortest mean time to detect. We also defined mean time between failure requirements for reference station antenna placement. Using these values of mean time to detect and mean time between failures, the airborne system is able to evaluate its integrity risk for comparison to requirements. We demonstrated how such a monitor works for an example shipboard landing application at different locations and satellite constellations with minimal impact on the availability.

ACKNOWLEDGMENT

The authors gratefully acknowledge the Naval Air Systems Command (NAVAIR) of the US Navy for supporting this research. However, the opinions presented in this paper are those of the authors and do not necessarily represent those of NAVAIR or any other affiliated agencies.

REFERENCES

[1] Sayim, I., Pervan, B., "LAAS Ranging Error Overbound for Non-Zero Mean and Non-Gaussian Multipath Error Distributions," *Proceedings of the 59th Annual Meeting of The Institute of Navigation and CIGTF 22nd Guidance Test Symposium*, Albuquerque, NM, June 2003, pp. 490-499.

[2] Khanafseh, S., Langel, S., Chan, F-C., Joerger, M., Pervan, B., "Monitoring Measurement Noise Variance for High Integrity Applications," *Proceedings of the 2012 International Technical Meeting of The Institute of Navigation*, Newport Beach, CA, January 2012, pp. 1157-1163.

[3] Lee, Jiyun, Pullen, Sam, Xie, Gang, Enge, Per, "LAAS Sigma-Mean Monitor Analysis and Failure-Test Verification," *Proceedings of the 57th Annual Meeting of The Institute of Navigation*, Albuquerque, NM, June 2001, pp. 694-704.

[4] Pullen, S., Lee, J., Xie, G., Enge, P., "CUSUM-Based Real-Time Risk Metrics for Augmented GPS and GNSS," *Proceedings of the 16th International Technical Meeting of the Satellite Division of The Institute of Navigation (ION GPS/GNSS 2003)*, Portland, OR, September 2003, pp. 2275-2287.

[5] Lee, Jiyun, Pullen, Sam, Enge, Per, "Sigma-Mean Monitoring for the Local Area Augmentation of GPS," *IEEE Transaction on Aerospace and Electronic Systems Vol. 42, No. 2, April 2006, pp. 625-635*.

[6] D. Hawkins and D. Olwell, *Cumulative Sum Charts and Charting for Quality Improvement*, New York: Springer-Verlag, 1998.

[7] M. Basseville and I. Nikiforov, *Detection of Abrupt Change: Theory and Application*. Englewood Cliffs, N.J. Prentice-Hall, 1993.

[8] S. Khanafseh and B. Pervan, "A New Approach for Calculating Position Domain Integrity Risk for Cycle Resolution in Carrier Phase Navigation Systems," *IEEE Transactions on Aerospace and Electronic Systems*, Vol. 46, No. 1, January 2010, pp. 296-307.

[9] P. Teunissen, D. Odijk, and P. Joosten, "A Probabilistic Evaluation of Correct GPS Ambiguity Resolution," *Proceedings of the 11th International Technical Meeting of the Satellite Division of the Institute of Navigation*, Nashville, TN, Sept. 1998.

[10] "Minimum Operational Performance Standards for Global Positioning System/Wide Area Augmentation System Airborne Equipment," RTCA Document Number DO-229C, Nov. 2001, Appendix B.5.

[11] M. B. Heo, "Robust Carrier Phase DGPS Navigation for Shipboard Landing of Aircraft," Ph.D. Dissertation, Illinois Institute of Technology, Chicago, IL, Dec. 2004.

[12] S. Khanafseh, "GPS Navigation Algorithms for Autonomous Airborne Refueling of Unmanned Air Vehicles," Ph.D. Dissertation, Illinois Institute of Technology, Chicago, IL, May 2008.

[13] S. Langel, S. Khanafseh, F. C. Chan, B. Pervan, "Cycle Ambiguity Reacquisition in UAV Applications using a Novel GPS/INS Integration Algorithm," *Proceedings of the 2009 International Technical Meeting of the Institute of Navigation ION-ITM 2009*, Anaheim, CA, Jan. 2009.

[14] G. A. McGraw, "Generalized Divergence-Free Carrier Smoothing with Applications to Dual Frequency Differential GPS," *NAVIGATION: Journal of Institute of Navigation*, Vol. 56, No. 2, Summer 2009.

[15] P. Misra and P. Enge, *Global Positioning System signals, Measurements, and Performance*. Lincoln, MA: Ganga-Jamuna Press, 2001.

[16] S. Wu, S. Peck, R. Fries, "Geometry Extra-Redundant Almost Fixed Solutions: A High Integrity Approach for Carrier Phase Ambiguity Resolution for High Accuracy Relative Navigation," *Proceedings of IEEE/ION PLANS 2008, Monterey*, CA, May 2008, pp. 568-582.